Original Article

Institution of MECHANICAL ENGINEERS
Journal of MECHANICAL ENGINEERING SCIENCE

Experimental investigation of ground effects on aerodynamics of sinusoidal leading-edge wings

Proc IMechE Part C:
J Mechanical Engineering Science
0(0) 1–14

DOI: 10.1177/0954406220975422
journals.sagepub.com/home/pic
SAGE

AA Mehraban and MH Djavareshkian

Abstract

Sinusoidal leading-edge wings have attracted many considerations since they can delay the stall and enhance the maneuverability. The main contribution of this research study is to experimentally investigate effects of ground on aerodynamic performance of sinusoidal leading-edge wings. To this end, 6 tubercled wings with different amplitudes and wavelengths are fabricated and compared with the baseline wing which has smooth leading-edge. Proposed wings are tested in different distances from the ground in a wind tunnel lab for a wide range of angle of attack from 0° to 36° and low Reynolds number of 45,000. Results indicated that lift coefficient is improved when wings get close to the ground. Furthermore, increment of protuberance amplitude in the vicinity of the ground could efficiently prevent stalling particularly for shorter wavelength.

Keywords

Sinusoidal leading-edge, ground effect, low Reynolds number, experimental aerodynamics, micro aerial vehicles, flow control

Date received: 4 July 2020; accepted: 30 October 2020

Introduction

Scientists in the field of aerospace engineering have always been discovering new techniques to improve the aerodynamic performance of aerial vehicles. Hence, some of them draw inspiration from wing shape of birds or marine animals because they believe natural creatures by far have the best performance.[1] Therefore, the field of bio-inspired engineering was established to bridge the gap between performance of natural creatures and manmade robots.

To this end, locomotion of humpback whale has grabbed many attentions in last decade due to its high maneuverability. Scientists have attributed this excellent performance to its wing shape which has sinusoidal leading-edge. Therefore, many studies have been done to reveal the secrets behind this especial geometry. These investigations have been conducted in different fields of study like wind turbines,[2] hydrofoils,[3] compressors,[4] noise reduction[5,6] and etc.

With regards to aerospace engineering, Johari et al.[7] were the first research group who focused on airfoils with sinusoidal leading-edge. They constructed their wings in different amplitudes and wave lengths and compared their aerodynamic performance to conventional wing with smooth leading-edge. They revealed that modified foils have higher lift coefficient by as much as 50% than unmodified one after stall point. Moreover, bio-inspired wings could noticeably delay the stall. They also showed that the protuberance amplitude plays significant role in lift and drag coefficients. This superior performance motivated other researchers in this research area to concentrate more on sinusoidal leading-edge wings. Zverkov et al.[8] concluded that the main discrepancy between wavy and conventional wings is related to their different boundary layer structures. Therefore, experimental study was performed to elucidate the boundary layer parameters at zero degree angle of attack and $Re = 1.7 \times 10^{5}$. They showed that the laminar-turbulent transition for peaks is observed at 30% of the chord downstream in comparison with troughs. Goruney and Rockwell[9] experimentally analyzed the flow field around the delta wing with sinusoidal leading-edges at $Re = 1.5 \times 10^{4}$. Results indicated that modified wing with amplitude of four percent of chord can considerably eliminate the large scale three dimensional separation observed in smooth leading-edge wing. More detail about flow

Department of Mechanical Engineering, Ferdowsi University of Mashhad, Mashhad, Iran

Corresponding author:
MH Djavareshkian, Department of Mechanical Engineering, Ferdowsi University of Mashhad, P.O. Box 9177948974, Mashhad, Iran.
Email: javareshkian@um.ac.ir

structure around the sinusoidal leading-edge delta wing can be found in.[10]

Hansen et al.[11] assessed the aerodynamic performance of sinusoidal leading-edge airfoils with different profiles. Similar to Johari et al.,[7] they deduced that a higher maximum lift coefficient and larger stall angle is obtained by the wing with less protuberance amplitude. Fluid flow around a NACA63_4-021 airfoil with sinusoidal leading-edge protuberances was numerically simulated by Dropkin et al.[12] They pointed out that low-pressure pockets in the troughs are formed on the modified airfoil, persisting to high angles of attack. They explained that these low-pressure pockets cause an increase in lift coefficient after stall region. This is in agreement to what stated in.[13–15] Skillen et al.[16] emphasized that a secondary flow is formed near the region of minimum chord of the sinusoidal leading-edge wing at $Re = 1.2 \times 10^5$ due to the spanwise pressure gradient. This causes higher-momentum fluid to be transferred toward the region behind the maximum chord. Consequently, the boundary layer is energized and stall is delayed. Performance of sinusoidal leading-edge wings with low aspect ratio was examined by Guerreiro and Sousa[17] in low Reynolds numbers. They highlighted that superiority of the sinusoidal leading-edge wings can be extended to low angles of attack by low Reynolds number flow. By conducting experimental study on swept smooth and tubercled NACA0021 wings, Bolzon et al.[18] manifested that sweeping changes the symmetry among counter rotating, streamwise vortex pairs. As a consequence, one vortex in each vortex pair becomes 4 times stronger than other one. In another research study,[19] they showed that sweeping the sinusoidal leading-edge wing reduces the lift to drag ratio after stall region. Research studies concerning sinusoidal leading-edge wings have been reviewed by Aftab et al.[20] from aerodynamic point of view.

More recently, Sinusoidal and spherical leading-edge NACA4415 airfoils were numerically compared with each other in different amplitudes and wave lengths. Results indicated that spherical leading-edge airfoils improve the aerodynamic performance higher than sinusoidal leading-edge airfoils. Investigating the effects of a single protuberance terminating at the tip of a swept wing on aerodynamic performance was the goal of Bolzon et al.[21] study. They tested the models in prestall angles of attack and concluded that single tubercle has no significant effects on aerodynamic coefficients. Similar study was done in[22] to analyze the effects of a single tubercle at about the middle of the span.

Cai et al.[23] focused on the role of periodic and aperiodic flow patterns in aerodynamics of sinusoidal leading-edge wings. To numerically simulate fluid flow around sinusoidal leading-edge wings, different approaches like LES[24,25] have been widely used. LES and DNS turbulence models were employed by Pérez-Torró and Kim[26] and Serson et al.[27] to simulate the flow around the sinusoidal leading-edge NACA0021 airfoil at $Re = 1.5 \times 10^4$. LES approach was employed by Pendar et al.[28] to study cavitating flow around a 3-D hydrofoil with a wavy leading-edge. Results indicated that flow separation is prevented by early development of the laminar separation bubble on the suction side of the wavy leading-edge hydrofoil. By using computational fluid dynamics, Rostamzadeh et al.[29] discovered the aerodynamic performance of sinusoidal leading-edge wings in transitional and turbulent Reynolds numbers. They showed that baseline wing has gradual stall and generates higher lift compared to the tubercled foil. Therefore, they emphasized that effects of Reynolds number should be taken into consideration by engineers. Effects of sinusoidal protuberances on tapered swept-back wings were analyzed by Wei et al.[30] Sudhakar et al.[31] experimentally compared the aerodynamic performance of a smooth leading-edge wing with a tubercled leading-edge wing with variable amplitude and wavelength along the span. They showed that tubercled wing with variable amplitude and wavelength has the highest performance. By conducting experimental measurement, Heesu et al.[32] and Post et al.[33] provided new insight into the physics of fluid around the bio-inspired sinusoidal leading-edge wings. Effects of low Reynolds number flows on aerodynamics of a NACA0012 wing with sinusoidal leading-edge were experimentally evaluated by Yasuda et al.[34] Similar to Guerreiro and Sousa,[17] they clarified that favorable effects of sinusoidal leading-edge wings are extended to low angles of attack by low Reynolds number flow. Authors recently investigated the role of smart flaps in the aerodynamic performance of sinusoidal and smooth leading-edge wings. Results showed that the stall angle could be further delayed by adding a smart flap to the trailing-edge of the sinusoidal leading-edge wing.[35]

On the other hand, it has been proven that aerodynamic performance of marine devises,[36] aerial vehicles[37] and race cars[38] is affected in the vicinity of the ground, named as ground effect. This is because that downwash velocity is reduced in the vicinity of the ground. As a result, drag coefficient decreases while effective angle of attack increases. These in turn lead to higher lift to drag coefficient ratio.[39] Johansson et al.[40] have shown why bats would like to fly in the ground proximity. They found that the aerodynamic power of bats could be reduced by 29% when they fly near the ground. An experimental study was performed by Jung et al.[41] to investigate aerodynamic coefficients of a NACA6409 airfoil in the vicinity of the ground over a wide range of angles of attack, aspect ratios and ground clearances. They concluded that the lift to drag ratio increases in low ground clearances and the center of pressure is moved toward the leading-edge. The ground effects on aerodynamic performance of smart flaps were numerically investigated by authors

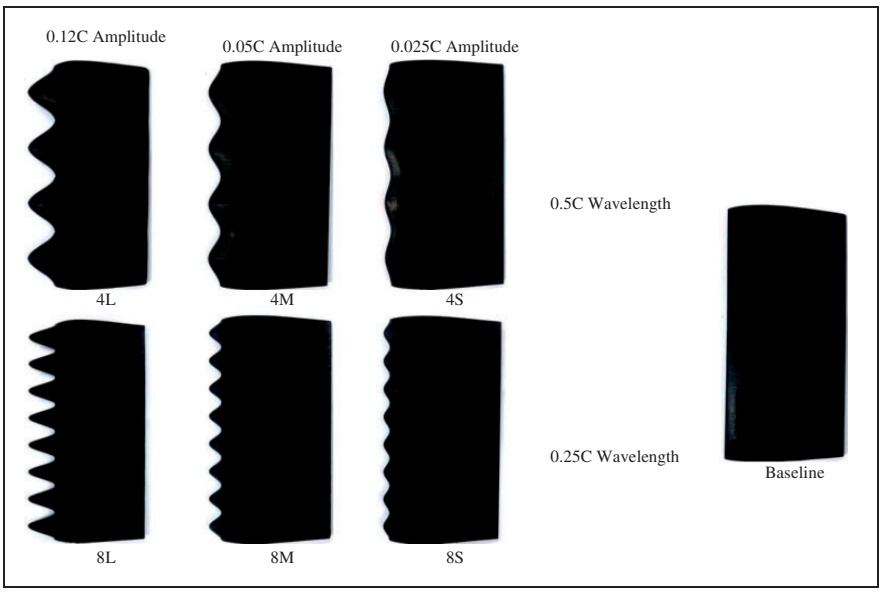

Figure 1. Manufactured wings.

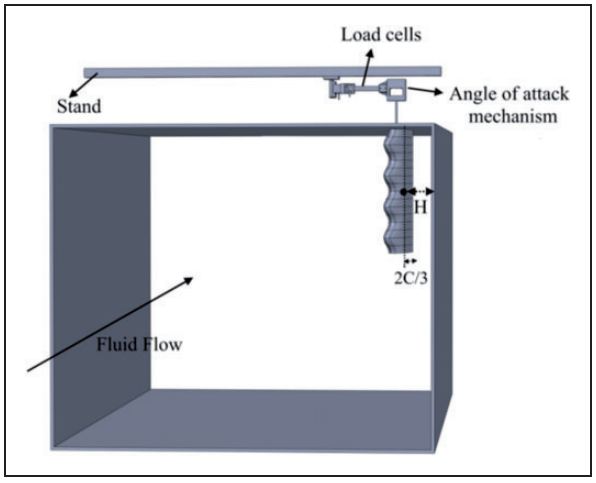

Figure 2. Schematic of the wing inside the wind tunnel.

in two and three dimensions.[37,39] Results showed that the tip vortex of the flap and wing is diminished in a low ground clearance. In another research study, authors studied the physics of fluid around an oscillating hydrofoil near water free surface.[36]

To the authors' knowledge, effects of ground on aerodynamic forces as well as stall angle of the sinusoidal-leading wings have not been analyzed yet. Therefore, the main objective of the present study is to experimentally investigate aerodynamics of sinusoidal leading-edge wings in the vicinity of the ground. To this end, six modified wings with different wavelengths and amplitudes are fabricated and are compared to unmodified or smooth leading-edge wing. Aerodynamic forces of these wings are measured and compared with each other in different distances from the ground for a wide range of angles of attack, ranging from 0° to 36°, and low Reynolds number of 45,000. This analysis is truly critical since

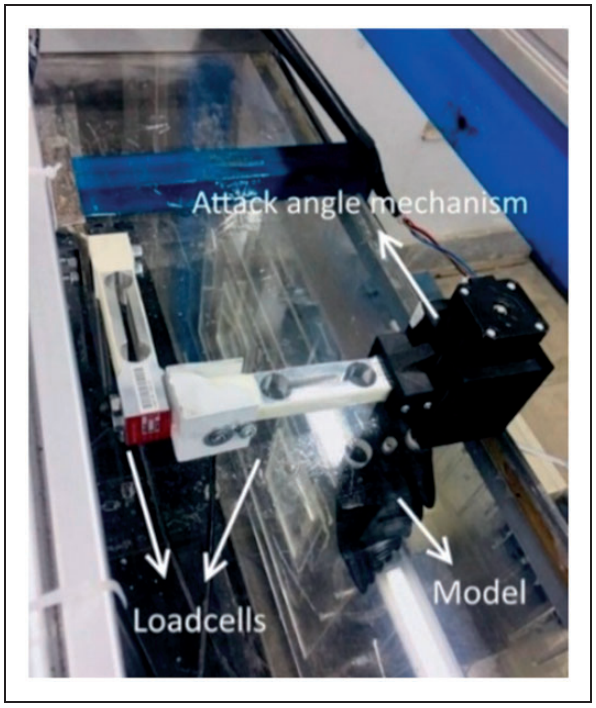

Figure 3. Designed and manufactured setups for load cells and attack angle adjustment.

most micro aerial vehicles fly in this flow regime. Moreover, as Zhang et al.[42,43] clarified, leading-edge protuberances as a flow control method act similarly to low profile vortex generator technique. However, using classical flow control method like vortex generators and also boundary layer suction[44] or thermal camber[45] for MAVs are very energy consuming and also lead to weight penalty. Therefore, using sinusoidal leading-edge protuberances as a passive flow control method would be a remarkable achievement and brings a lot of benefits.

Experimental setup

Preparation of wings

All the wings tested in this study are demonstrated in Figure 1. Mean chord and span of all wings are 10.2 cm and 20.4 cm, respectively. Six wings have sinusoidal leading-edge with different amplitudes of 0.025 C, 0.05 C, and 0.12 C and two wavelengths of 0.25 C and 0.50 C. As Johari et al.[7] sated, these contents for wavelength and amplitude stay within the range of the humpback whale flippers. The leading edge of seventh wing is smooth and is considered as base line wings. All wings have NACA63_4-021 profile and were firstly designed in SolidWork software and then fabricated by a 3-D printer. All wings are hand polished after construction and their surface roughness height is much less than the critical roughness height mentioned by Custodio et al.[46]

Wind tunnel and measurement instruments

The experiments are carried out in an open circuit, low speed, and closed test section wind tunnel with a test section of 120 cm × 100 cm. The turbulence intensity of the wind tunnel is 0.3% at a velocity of 5 m/s. This value for turbulence intensity is much less than that mentioned by Mueller.[47] Experiments are performed for a wide range of angle of attack from 0° to 36°. Furthermore, velocity for this research study was set to 7.6 m/s. Therefore, associated Reynolds number based on this freestream velocity and mean chord length is equal to 45,000.

To investigate the effects of ground on aerodynamic forces of sinusoidal leading-edge wings, proposed wings are tested in different distances from the wind tunnel wall. To this end, normalized number of H/C is used to show these distances, where C is the mean chord of the wing and H is the distance between

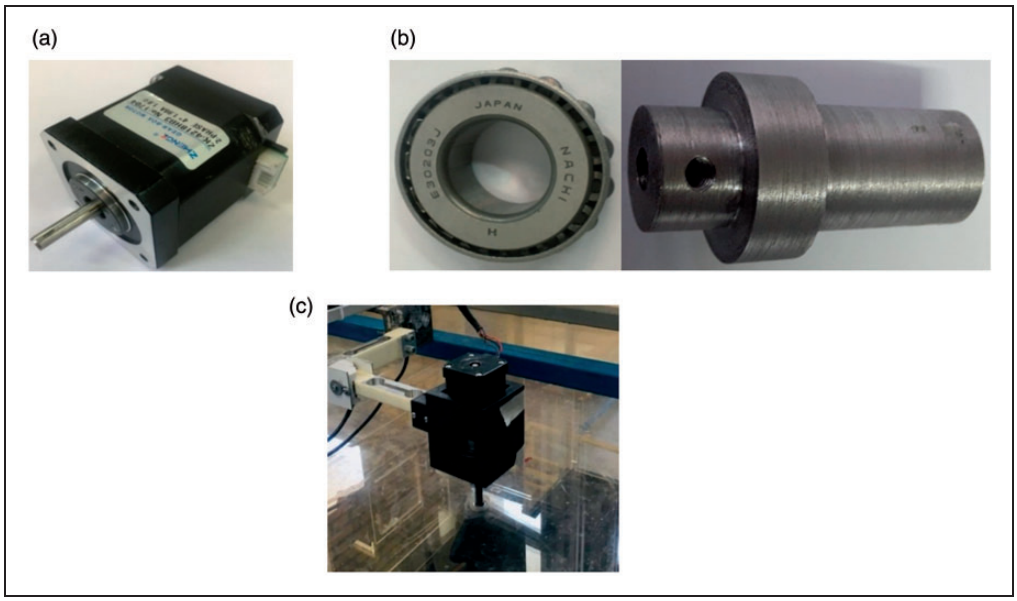

Figure 4. Views of Angle of attack mechanism; (a) stepper motor, (b) radial roller bearing, and (c) shield.

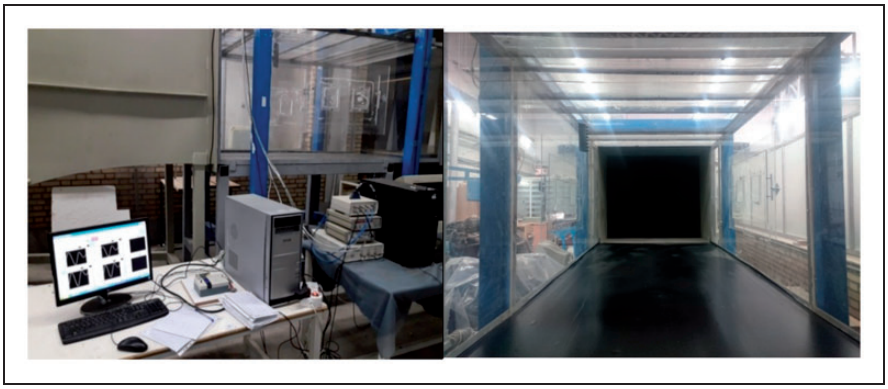

Figure 5. The model inside the wind tunnel.

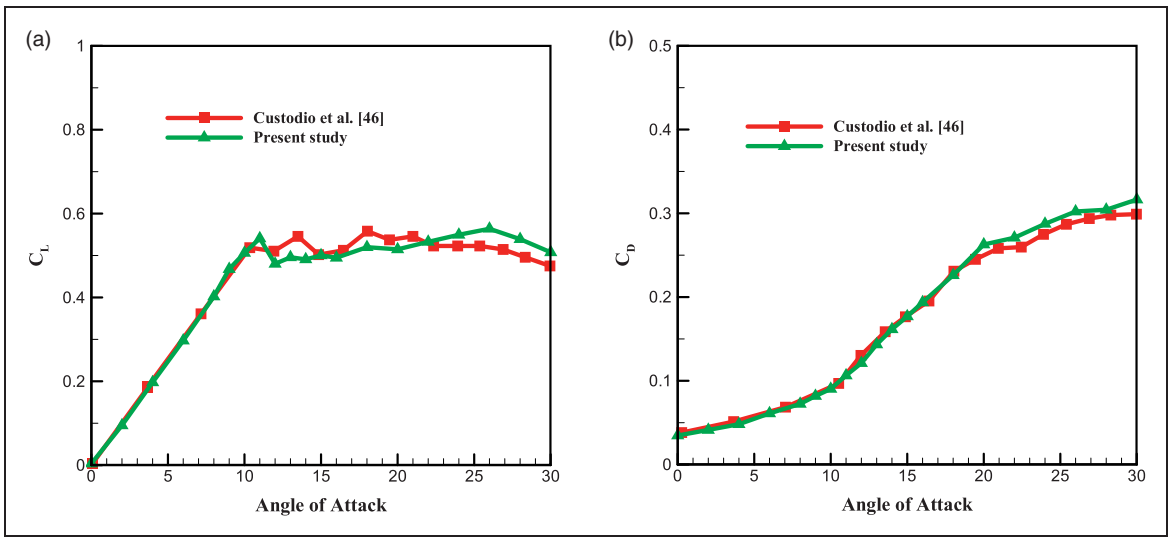

Figure 6. Comparison between aerodynamic coefficients of this study and those of Custodio et al. [46] (a) lift coefficient, and (b) drag coefficient versus angle of attack.

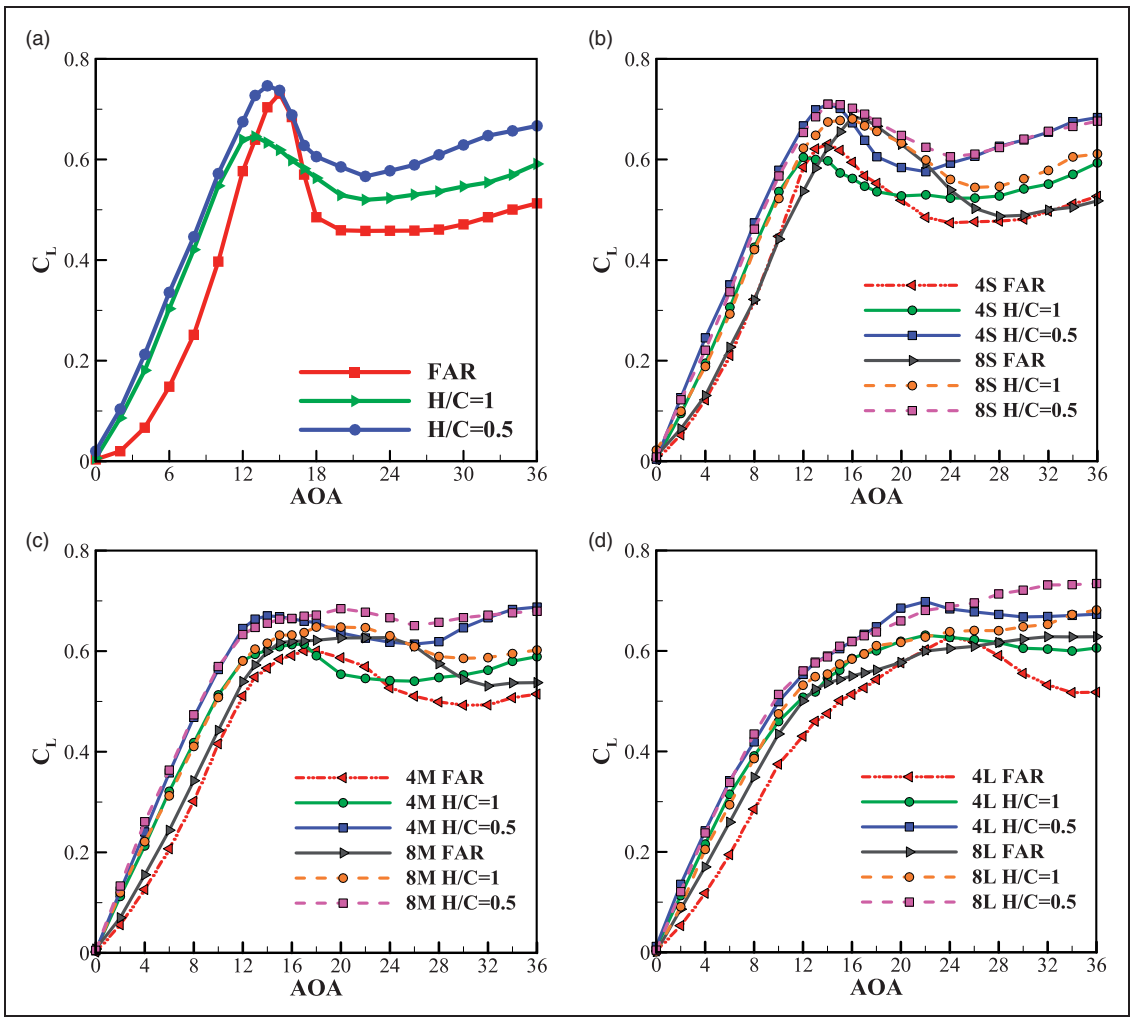

Figure 7. Variation of lift coefficient with angle of attack for different distances to ground (a) baseline (b) 4S and 8S (c) 4 M and 8 M (d) 4 L and 8 L.

chord of the wing and wall. According to Figure 2, H is defined at last two-thirds of the chord at mid span. Wings are tested in three H/Cs of 0.5, 1 and ∞ to reveal the effects of ground.

Two one-dimensional strain gauge load cells (model Bongshin OBU-N49106 and OBU-N50170) are employed to measure the lift and drag forces.[48] The relative error of these force sensors is below 0.4%. The hysteresis, non-repeatability, and non-linearity of force sensors are less than 0.02% of full scale (3 kg and 6 kg).[49] The relative uncertainty in force coefficients was determined to be less than 1%. According to Figure 3, the load cells are connected to a stepper motor (model ZhengKe motor ZGA42FH) and a stand at the top of the wind tunnel. As shown, load cells are placed in the right position. The mechanism of attack angle adjustment is represented in Figure 4. In this mechanism, the stepper motor (Figure 4(a)) is implemented to convert the rotational motion of the electrical motor to the

Table 1. Lift characteristics of wings at different ground clearances.

	$dC_L/d\alpha$ (per deg)			$C_{L\,max}$			α at $C_{L\,max}$(deg)		
Wing	H/C = 0.5	H/C = 1	H/C=∞	H/C = 0.5	H/C = 1	H/C=∞	H/C = 0.5	H/C = 1	H/C=∞
4S	0.057	0.053	0.044	0.710	0.604	0.630	14	12	14
4M	0.056	0.051	0.041	0.670	0.614	0.601	14	17	17
4L	0.049	0.045	0.037	0.698	0.631	0.629	22	22	24
8S	0.056	0.050	0.044	0.711	0.681	0.684	14	16	16
8M	0.056	0.050	0.044	0.684	0.648	0.627	20	18	24
8L	0.051	0.047	0.043	0.734	0.682	0.628	36	36	36
Baseline	0.055	0.053	0.040	0.746	0.646	0.731	14	13	15

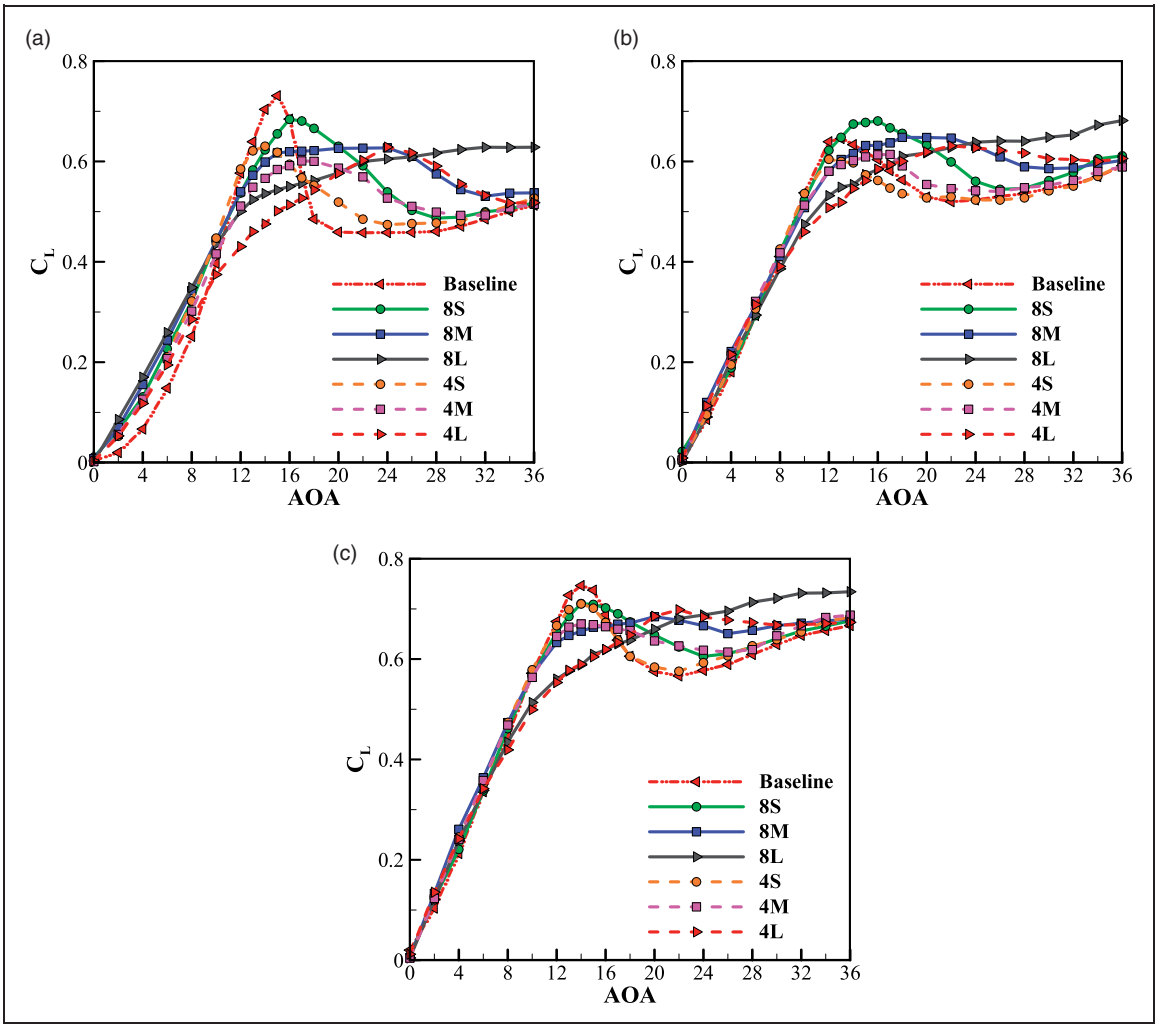

Figure 8. Variation of lift coefficient with angle of attack for different wings (a) H/C=∞ (b) H/C = 1 (c) H/C = 0.5.

wings via a radial roller bearing (Figure 4(b)). These components are assembled and then placed into a shield which can be seen in Figure 4(c). Forces are acquired for 50 seconds for each case at 1000 Hz. Known weights are used for calibrating the load cells. The output functions are used to convert the average measured signals to force. The measured voltage by the load cell will be amplified by using an amplifier (model Dacell DN-AM100). All the signals are acquired by a data acquisition board (model Advantech PCI-1710HG). The model inside the wind tunnel is depicted in Figure 5.

As shown in our previous experimental work, in the worst case, i.e. the lowest Reynolds number (Re = 29,000), about 2.95% of the wing is in the wind tunnel boundary layer.[35] This content is less than that of Custodio et al.[46] where the wind tunnel boundary layer covers 4.3 and 7.8% of the model span for the largest and smallest freestream velocities, respectively.

Validation

Lift and drag coefficients of the wing with sinusoidal leading-edge (4L) at Reynolds number of 90,000 are compared to those of Custodio et al.[46] and represented in Figure 6. As shown, there would be an acceptable agreement between outcomes of present experimental work and those of Custodio et al.[46] The average error between lift and drag coefficients of the present study and data of Custodio et al.[46] is 3.7% and 3.9%, respectively.

Results and discussion

Results are analyzed and discussed in different distances from the ground to reveal how ground affects the aerodynamics of sinusoidal leading-edge wings. Since both sinusoidal leading-edge protuberances and ground individually have positive effects on aerodynamics of wings, it would be interesting to measure and analyze aerodynamic forces when both of them are exploited.

Lift coefficient

In order to understand the effects of ground precisely, performance of each wing is analyzed in detail. To this end, lift coefficient of the wings with wavelength

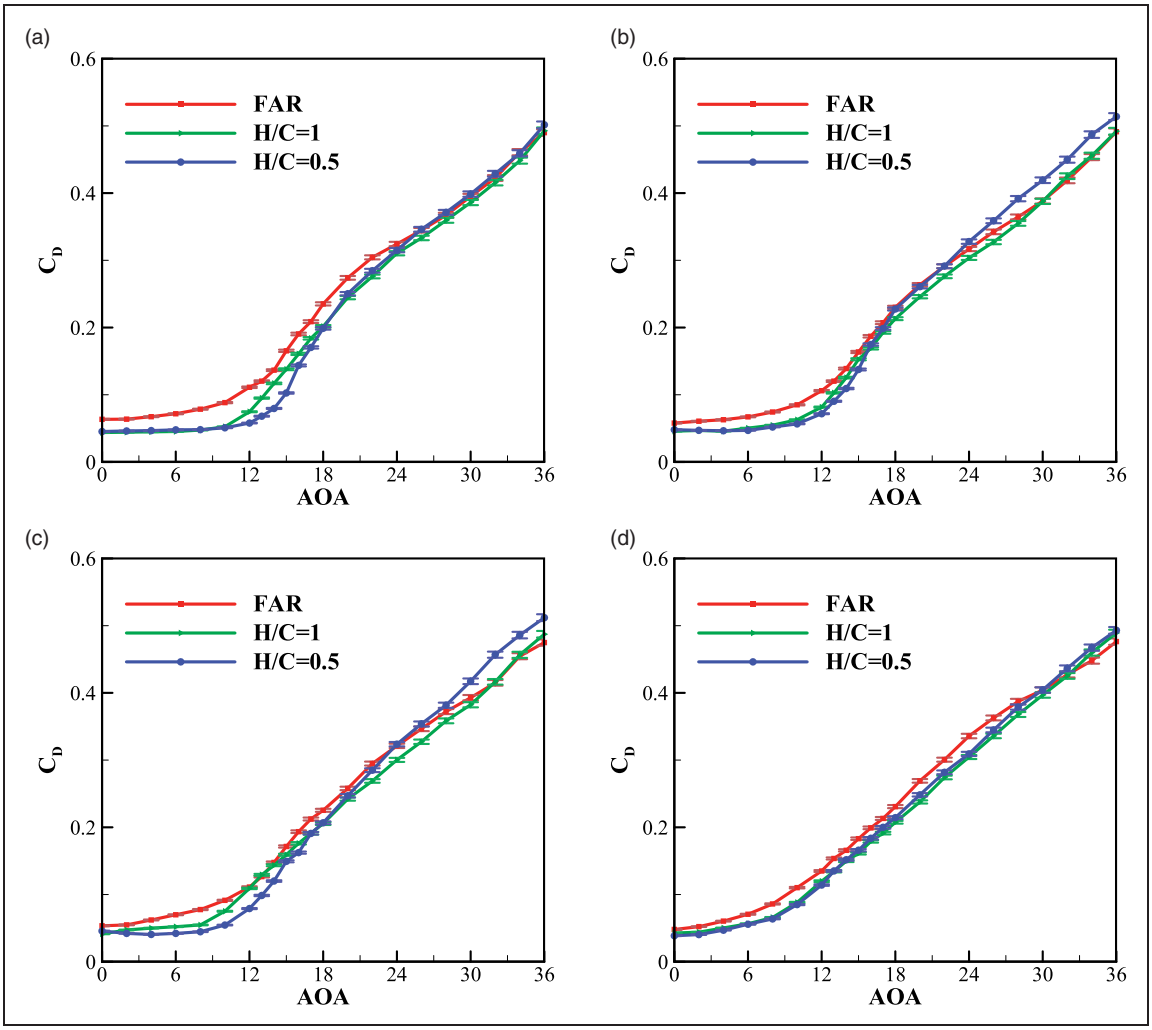

Figure 9. Variation of drag coefficient with angle of attack for different distances to ground (a) baseline (b) 4S (c) 4M (d) 4L.

of 0.5 C is illustrated in Figure 7 for different H/Cs. According to this figure, the best scenario for all wings occurs at H/C = 0.5, where the lift coefficient is higher than other H/Cs in all angles of attack. This is because that pressure in lower surface of the wings is higher due to the ram pressure.[39] The maximum pressure happens at the leading-edge (stagnation point) and due to converge-diverge shape between wing lower surface and the ground, pressure firstly decreases and then increases. This consequently makes a pressure difference around the wing and produces higher lift than the wing far from the ground. However, the content of this improvement is different for proposed wings. 4 L wing is the most tubercled benefited wing.

Furthermore, the trend of lift coefficient diagrams is changed with increment of amplitude. 4 M and 4 L wings do not stall in the same manner as the baseline wing with the smooth leading-edge and also the 4S wing in the vicinity of the ground. In other words, the lift coefficient of former does not decrease as intense as later. Therefore, 4 M and 4 L wings experience a really smoother stall than the baseline wing and also 4S wing at H/C=∞. As concluded in the literature, sinusoidal leading-edge wings delay the stall point. However, it is revealed in this paper that this type of wings in the vicinity of the ground prevent stalling. This would be so valuable since it can help aerial vehicles to have high maneuverability. It should be mentioned that sinusoidal leading-edge wings have less maximum lift coefficient than baseline wing.

According to Figure 7, lift coefficient of 8S, 8 M and 8 L wings enhances when the wings reach the ground. However, this enhancement in lift coefficient is less sensible compared to the wings with 0.5 C wavelength. The highest improvement belongs to 8S wing. Moreover, the behavior of lift coefficient along angle of attack for tubercled wings is changed with amplitude. While 8S wing stalls and 8 M wing reaches a plateau, lift coefficient of 8 L wing has an upward trend with angle of attack.

Lift characteristics of proposed wings are tabulated in Table 1 based on different ground clearances. Therefore, performance of all wings can be compared with each other. The slope of lift curve, $dC_L/d\alpha$, is calculated for $0^\circ \leq$AOA$\leq 10^\circ$ where almost all curves have linear behavior. This slope for all wings is enhanced when they get closer to ground. Similar to

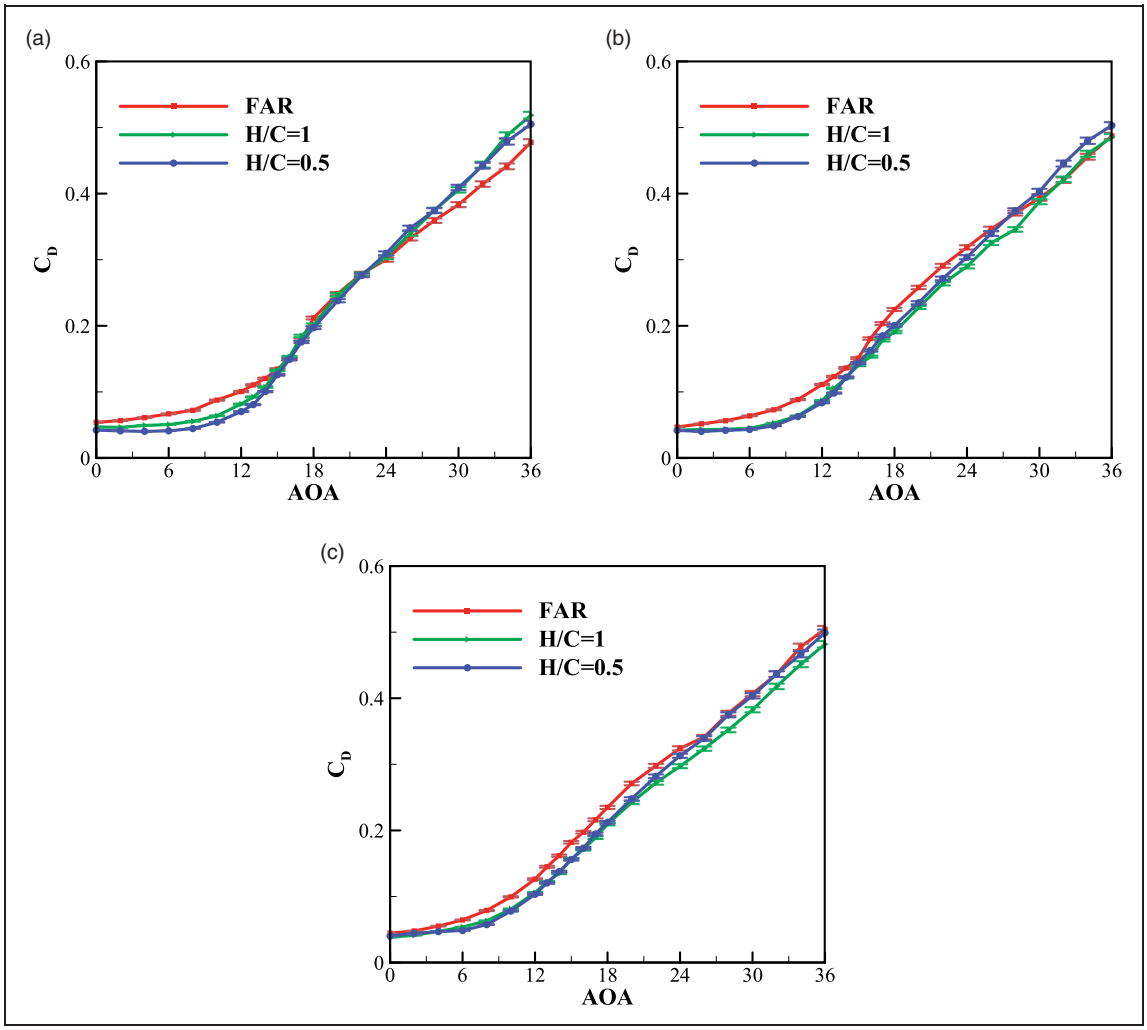

Figure 10. Variation of drag coefficient with angle of attack for different distances to ground (a) 8S (b) 8 M (c) 8 L.

Johari et al.,[7] lift curve slope is reduced with protuberance amplitude. Furthermore, maximum lift coefficient increases when the H/C is reduced except for shortest amplitude (4S and 8S). It is worth mentioning that the angle that maximum lift coefficient happens increases with amplitude for all H/Cs.

Lift coefficient of all seven wings is plotted in Figure 8 in order to be compared with each other for different ground clearances. In each H/C, reducing the wavelength generally increases the lift coefficient. This improvement is reduced when the wings get closer to the ground. However, clear behavior by changing the amplitude is not observed.

In Figure 8(a), the lift coefficient of all wings increases almost linearly for $\alpha \leq 9°$. As explained in,[14] this is because that in this range of angle of attack, the flow is almost attached to the wing surface. As a result, strong negative pressure region is formed near the leading-edge, leading to an increase in lift coefficient. After that, baseline wing produces the highest lift coefficient before stall angle. As Johari et al.[7] revealed, while the flow over first three quarter of the baseline wing is attached, it is separated over the half of the sinusoidal leading-edge wings. They pointed out that separation for modified wings occurs at troughs while flow on peaks is attached. Next, lift coefficient of some wings such as baseline, 4S and 8S drop suddenly. However, stall for 8S and 4S wings is much smoother than baseline wing. This can be attributed to the fully developed flow separation over these wings, resulting in significant reduction in lift coefficient. This point is known as stall point. Guerreiro and Sousa[17] clarified that bursting separation bubbles formed just before stall is the main factor contributing to rapid lift reduction after stall. In poststall region, the baseline wing has the least lift coefficient. This can be explained by separation region formed over the entire baseline wing. On the other hand, flow is attached over the leading-edge protuberances due to generation of longitudinal vortices and separation bubble. Subsequently, separation bubbles at the troughs form a negative pressure region, leading to an increase in lift coefficient.[34]

The lift coefficient of all wings is enhanced when ground clearance is reduced from ∞ to 1 in Figure 8 (b). An increase in protuberance amplitude of wings with shorter wavelength decreases this improvement while this is conversed for the wings with 0.5c wavelength. Furthermore, longer wavelength wings are more sensitive to ground clearance than other

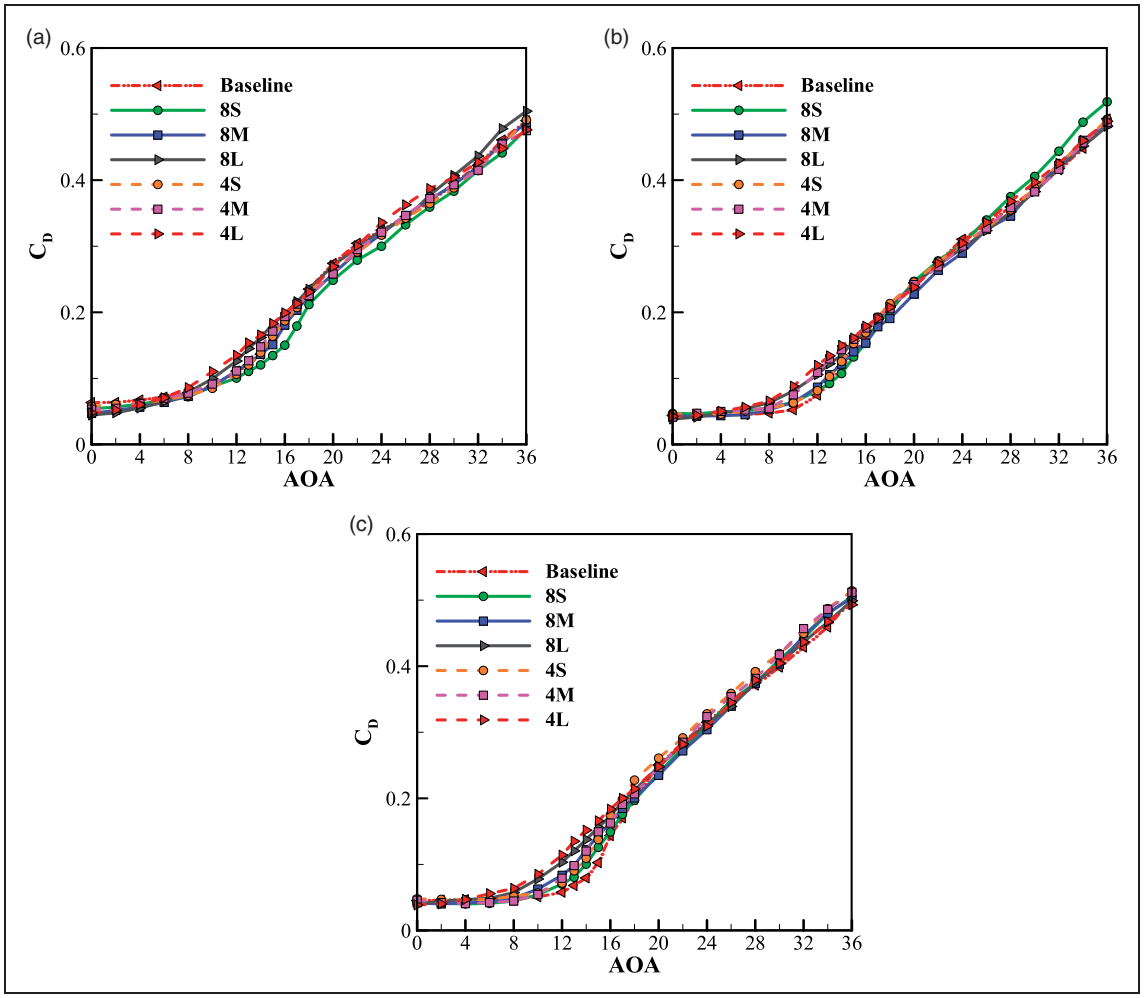

Figure 11. Variation of drag coefficient with angle of attack for different wings (a) H/C=∞ (b) H/C = 1 (c) H/C = 0.5.

wavelength. This improvement continues when the wings get further closer to the ground (H/C = 0.5).

Drag coefficient

Drag coefficient of wings with wavelength of 0.5 C is plotted in Figure 9. In Figure 9(b), the drag coefficient of 4S wing at H/C=∞ is slightly higher than other ground clearances for $\alpha \leq 18°$. However, 4S wing at H/C = 0.5 produces relatively higher drag compared to other ground clearances for $\alpha \geq 18°$. Furthermore, there is an increase in drag coefficient for $12° \leq \alpha \leq 18°$. This behavior is observed in baseline and 4 M wings in Figure 9(a) and (c) as well. This behavior can be explained by results of previous study published by authors.[39] As known, drag coefficient is divided to two elements (1) pressure drag and (2) frictional drag. Pressure distribution at the lower surface of the wings increases when they get close to the ground, resulting in increment of pressure drag. Although the surface shear stress on the upper surface for all H/Cs is identical, shear stress distribution at the lower surface for the wing in the vicinity of the ground is less than that far from the ground for low angles of attack. Therefore, wings closer to the ground have less frictional drag.

On the other hand, for high angles of attack, shear stress distribution for lower and upper surfaces of wings is reduced when the wings get closer to the ground. Steep slope in drag coefficient, reported for baseline, 4S and 4 M wings, is not observed for 4 L wing. Furthermore, drag coefficient of this wing in the vicinity of the ground is almost less than that far from the ground until angle of attack of 30°.

Figure 10 represents the drag coefficient of wings with 0.25 C wavelength. The same behavior as the wings with 0.5 C wavelength is reported for mentioned wings. Therefore, it can be concluded that in contrast to lift coefficient, drag coefficient is less affected by wavelength.

Drag coefficient of all seven wings is illustrated in Figure 11 for different ground clearances. In each ground clearance, increasing the protuberance amplitude slightly grows the drag coefficient whereas drag coefficient a little goes up when wavelength increases.

In Figure 11(a), drag coefficient of sinusoidal leading-edge wings is slightly higher than smooth leading-edge one for $\alpha \geq 6°$. This can be justified by

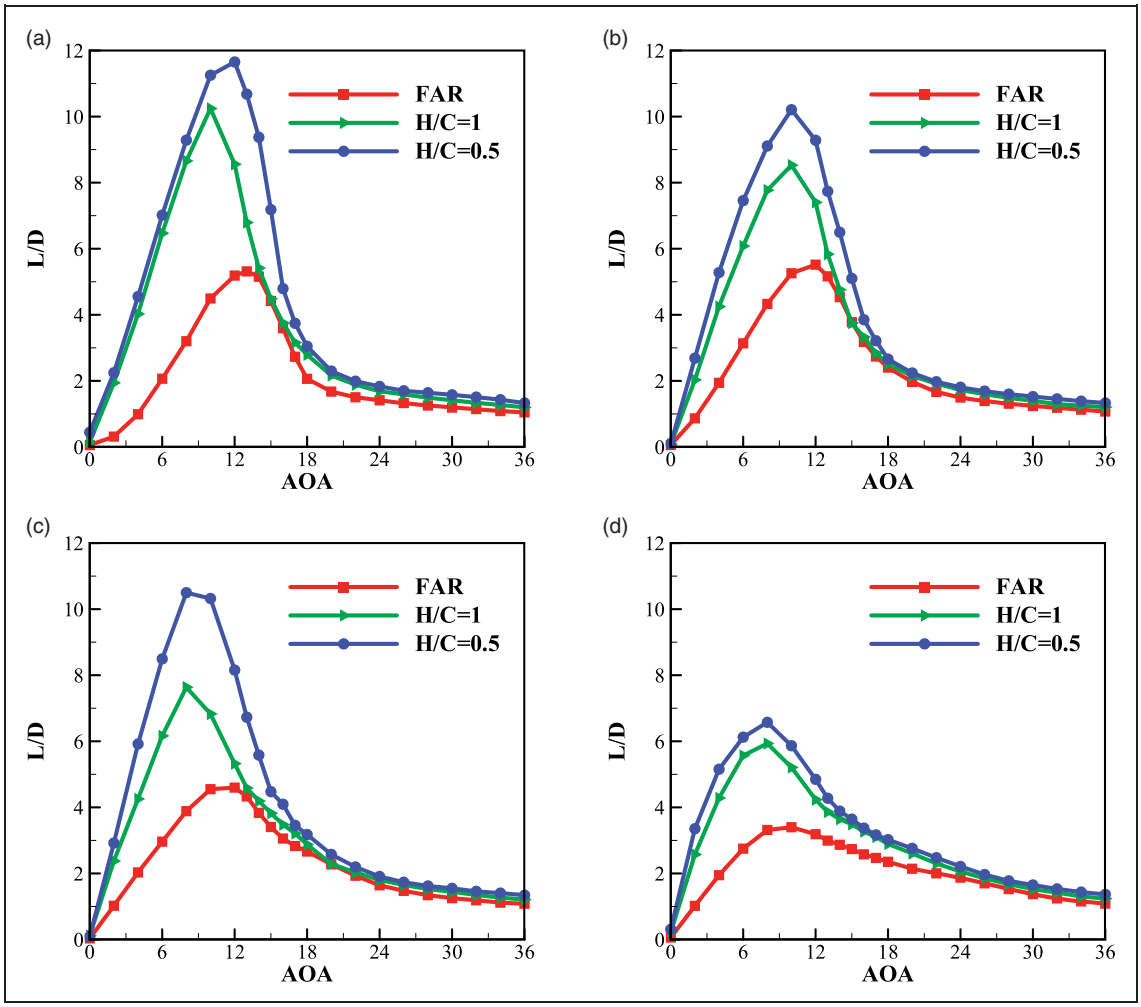

Figure 12. Variation of lift to drag ratio with angle of attack for different distances to ground (a) baseline (b) 4S (c) 4M (d) 4L.

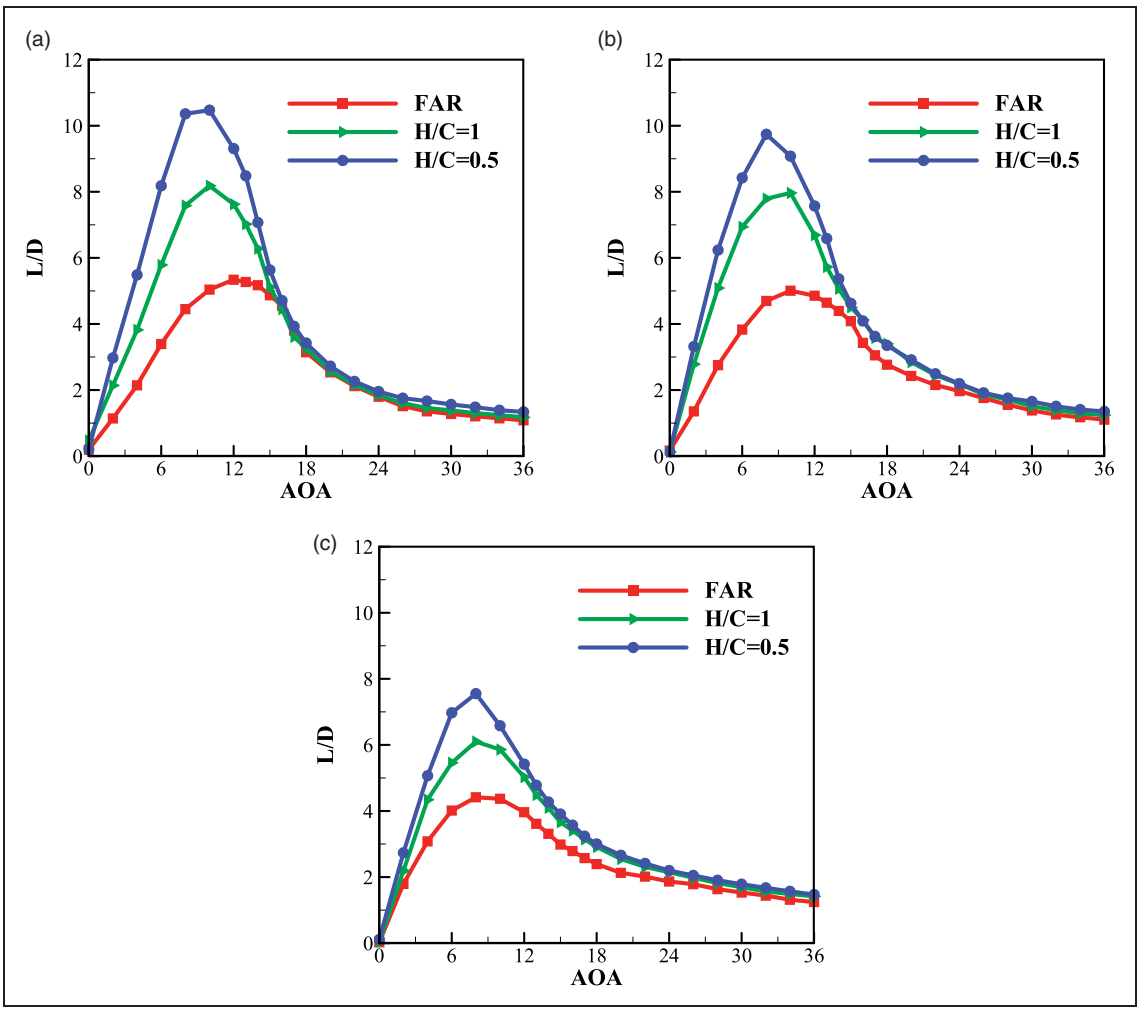

Figure 13. Variation of lift to drag ratio with angle of attack for different distances to ground (a) 8S (b) 8 M (c) 8 L.

Table 2 Lift to drag ratio characteristics of wings at different ground clearances.

	$(C_L/C_D)_{max}$			α at $(C_L/C_D)_{max}$ (deg)		
Wing	H/C = 0.5	H/C = 1	H/C=∞	H/C = 0.5	H/C = 1	H/C=∞
4S	10.21	8.53	5.52	10	10	12
4M	10.50	7.64	4.60	8	8	12
4L	6.57	5.93	3.39	8	8	10
8S	10.47	8.18	5.34	10	10	12
8M	9.74	7.96	5.01	8	10	10
8L	7.55	6.10	4.42	8	8	8
Baseline	11.65	10.25	5.32	12	10	13

existence of streamwise vortices, increasing surface shear stress.[15] However, all the wings almost produce identical drag coefficient in high angle of attack because they can be considered as a bluff.[7] In Figure 11(c), when the ground clearance decreases to H/C = 0.5, the drag coefficient is somewhat reduced.

Lift to drag ratio

Aerodynamic efficiency or lift to drag ratio is discussed in this section in order to better compare the overall performance of constructed wings. Therefore, this ratio for wings with 0.5 C wavelength is shown in Figure 12. Based on this figure, aerodynamic performance of all wings enhances when they get close to the ground. The maximum lift to drag ratio in each ground clearance belongs to smooth leading-edge wing. Among wings with 0.5 C wavelength, 4 M wing is the most benefited wing while 4 L wing is the least affected model. It should be noted that values of lift to drag ratio for all wings almost are identical for $\alpha \geq 18^\circ$

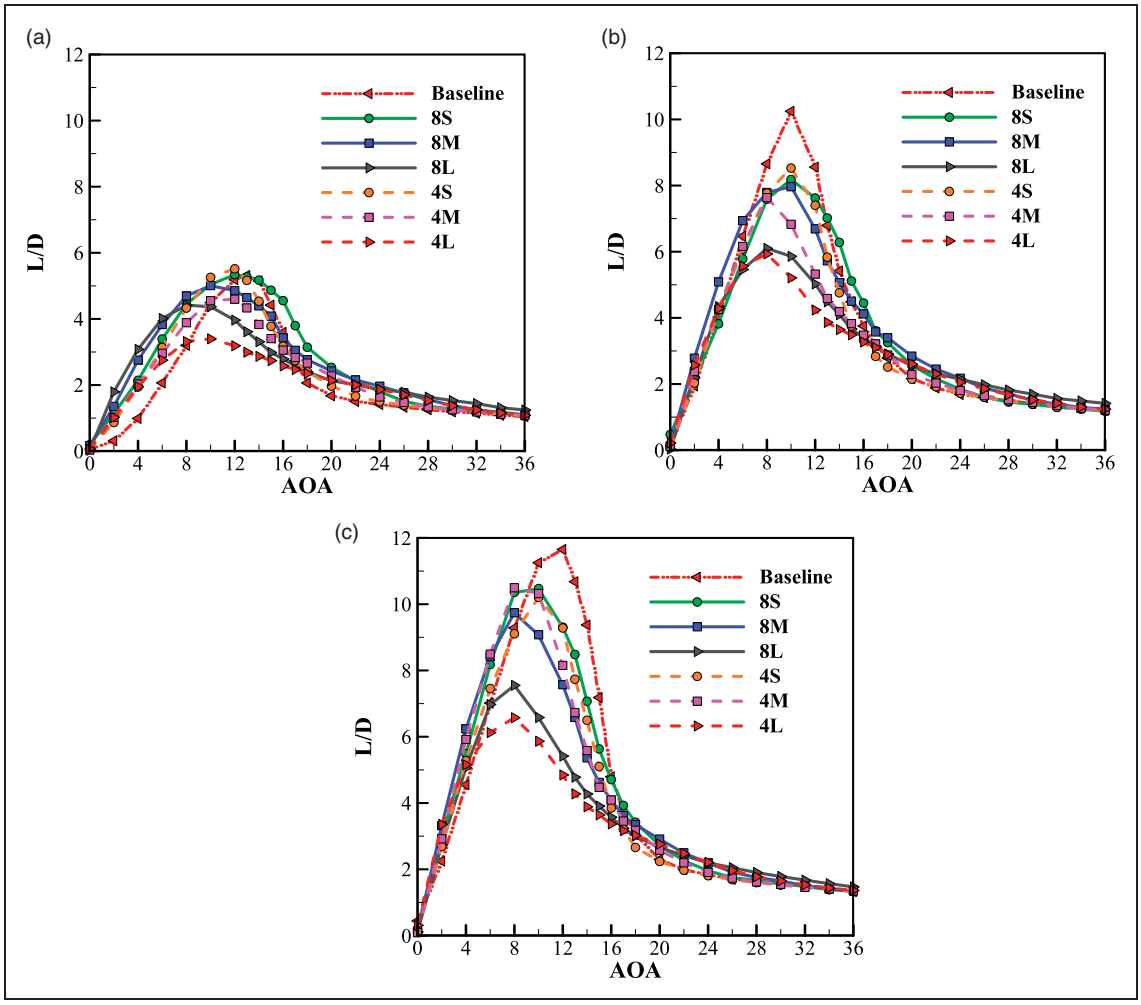

Figure 14. Variation of lift to drag ratio with angle of attack for different wings (a) H/C=∞ (b) H/C = 1 (c) H/C = 0.5.

Figure 13 describes the variation of lift to drag ratio for the wings with 0.25 C wavelength. According to this figure, the maximum aerodynamic efficiency is obtained at the closest distance to the ground for all wings. Furthermore, the maximum lift to drag ratio for almost all wings is advanced when H/C is reduced. Among wings with 0.25 C wavelength, 8S wing is introduced as the most affected wing, while 8 L wing has the least sensitivity.

Aerodynamic characteristics of the wings regarding to lift to drag ratio are shown in Table 2. Superiority of the ground effect can be concluded by this table. Reducing the ground clearance increases the maximum lift to drag ratio. Smooth leading-edge wing has the most improvement in maximum lift to drag ratio when it gets from H/C=∞ to H/C = 0.5. Among sinusoidal leading-edge wings, 4 M wing shows the highest improvement while the 8 L wing is the least affected one. Furthermore, maximum lift to drag ratio is generally reduced with increment of amplitude. However, as shown before, higher wing amplitude would be so beneficial since it delays the stall although it produces higher drag and decreases the maximum lift to drag ratio.

Lift to drag ratio for seven tested wings is demonstrated in Figure 14. As expected, a reduction in wavelength in each ground clearance generally improves the aerodynamic efficiency, since it could effectively reduce the drag and increase the lift coefficient.

Conclusion

This research study experimentally focused on the effects of ground on aerodynamics of sinusoidal leading-edge wings. Therefore, 6 wings with sinusoidal leading-edge with different amplitudes and wavelengths and one wing with smooth leading-edge were fabricated. Next, experiments were conducted in the wind tunnel for angle of attack, ranging from 0° to 36° and low Reynolds number of 45,000. Aerodynamic forces of proposed wings were measured for different distances from the ground and compared with each other. The main findings of present study are summarized as follows:

- Lift coefficient of all wings increases when the ground clearance is reduced.

- More lift coefficient is produced with shorter wavelength. This improvement is reduced when the wings get closer to the ground. Reduction of wavelength decreases the drag coefficient as well. Therefore, it can be considered as a desirable geometric trait.
- Increment of protuberance amplitude in the vicinity of the ground could efficiently prevent stalling particularly for shorter wavelength. However, it increases the drag coefficient.
- The slope of lift curve for all wings is enhanced when the ground clearance is reduced.
- In low angles of attack, drag coefficient of wings far from the ground is higher than in the vicinity of the ground. However, this behavior is conversed for high angles of attack.
- Aerodynamic efficiency of all wings is improved with a decrease in ground clearance. Among sinusoidal leading edge wings, 4M wing has the highest lift to drag ratio when it get closer to the ground.

Declaration of conflicting interests

The author(s) declared no potential conflicts of interest with respect to the research, authorship, and/or publication of this article.

Funding

The author(s) received no financial support for the research, authorship, and/or publication of this article.

ORCID iD

MH Djavareshkian https://orcid.org/0000-0003-1766-1190

References

1. Shyy W, Lian Y, Tang J, et al. *Aerodynamics of low Reynolds number flyers*. Cambridge: Cambridge University Press, 2007.
2. Wang Z, Wang Y and Zhuang M. Improvement of the aerodynamic performance of vertical axis wind turbines with leading-edge serrations and helical blades using CFD and Taguchi method. *Energy Convers Manag* 2018; 177: 107–121.
3. Custodio D, Henoch C and Johari H. Cavitation on hydrofoils with leading edge protuberances. *Ocean Eng* 2018; 162: 196–208.
4. Zheng T, Qiang X, Teng J, et al. Investigation of leading edge tubercles with different wavelengths in an annular compressor cascade. *Int J Turbo Jet-Engines* 2018.
5. Chen W, Qiao W, Tong F, et al. Experimental investigation of wavy leading edges on rod-aerofoil interaction noise. *J Sound Vibr* 2018; 422: 409–431.
6. Tong F, Qiao W, Chen W, et al. Numerical analysis of broadband noise reduction with wavy leading edge. *Chin J Aeronaut* 2018; 31: 1489–1505.
7. Johari H, Henoch CW, Custodio D, et al. Effects of leading-edge protuberances on airfoil performance. *AIAA J* 2007; 45: 2634–2642.
8. Zverkov I, Zanin B and Kozlov V. Disturbances growth in boundary layers on classical and wavy surface wings. *AIAA J* 2008; 46: 3149–3158.
9. Goruney T and Rockwell D. Flow past a delta wing with a sinusoidal leading edge: near-surface topology and flow structure. *Exp Fluids* 2009; 47: 321–331.
10. Chen H and Wang J-J. Vortex structures for flow over a delta wing with sinusoidal leading edge. *Exp Fluids* 2014; 55: 1761.
11. Hansen KL, Kelso RM and Dally BB. Performance variations of leading-edge tubercles for distinct airfoil profiles. *AIAA J* 2011; 49: 185–194.
12. Dropkin A, Custodio D, Henoch CW, et al. Computation of flow field around an airfoil with leading-edge protuberances. *J Aircr* 2012; 49: 1345–1355.
13. Rostamzadeh N, Kelso RM, Dally BB, et al. The effect of undulating leading-edge modifications on NACA 0021 airfoil characteristics. *Phys Fluids* 2013; 25: 117101.
14. Rostamzadeh N, Hansen KL, Kelso RM, et al. The formation mechanism and impact of streamwise vortices on NACA 0021 airfoil's performance with undulating leading edge modification. *Phys Fluids* 2014; 26: 107101.
15. Hansen KL, Rostamzadeh N, Kelso RM, et al. Evolution of the streamwise vortices generated between leading edge tubercles. *J Fluid Mech* 2016; 788: 730–766.
16. Skillen A, Revell A, Pinelli A, et al. Flow over a wing with leading-edge undulations. *AIAA J* 2015; 53: 464–472.
17. Guerreiro JLE and Sousa JMM. Low-Reynolds-number effects in passive stall control using sinusoidal leading edges. *AIAA J* 2012; 50: 461–469.
18. Bolzon MDP, Kelso RM and Arjomandi M. Formation of vortices on a tubercled wing, and their effects on drag. *Aerosp Sci Technol* 2016; 56: 46–55.
19. Bolzon MD, Kelso RM and Arjomandi M. Force measurements and wake surveys of a swept tubercled wing. *J Aerosp Eng* 2017; 30: 04016085.
20. Aftab SMA, Razak NA, Mohd Rafie AS, et al. Mimicking the humpback whale: an aerodynamic perspective. *Progr Aerosp Sci* 2016; 84: 48–69.
21. Bolzon MD, Kelso RM and Arjomandi M. Performance effects of a single tubercle terminating at a swept wing's tip. *Exp Therm Fluid Sci* 2017; 85: 52–68.
22. Cai C, Zuo Z, Liu S, et al. Effect of a single leading-edge protuberance on NACA 634-021 airfoil performance. *J Fluids Eng* 2018; 140: 021108.
23. Cai C, Zuo Z, Maeda T, et al. Periodic and aperiodic flow patterns around an airfoil with leading-edge protuberances. *Phys Fluids* 2017; 29: 115110.
24. Lar Kermani E, Roohi E and Porté-Agel F. Evaluating the modulated gradient model in large eddy simulation of channel flow with OpenFOAM. *J Turbul* 2018; 19: 600–620.
25. Zahiri A-P and Roohi E. Anisotropic minimum-dissipation (AMD) subgrid-scale model implemented in OpenFOAM: Verification and assessment in single-phase and multi-phase flows. *Comput Fluids* 2019; 180: 190–205.
26. Pérez-Torró R and Kim JW. A large-eddy simulation on a deep-stalled aerofoil with a wavy leading edge. *J Fluid Mech* 2017; 813: 23–52.
27. Serson D, Meneghini JR and Sherwin SJ. Direct numerical simulations of the flow around wings with spanwise waviness. *J Fluid Mech* 2017; 826: 714–731.

28. Pendar M-R, Esmaeilifar E and Roohi E. LES study of unsteady cavitation characteristics of a 3-D hydrofoil with wavy leading edge. *Int J Multiph Flow* 2020; 132: 103415.
29. Rostamzadeh N, Kelso RM and Dally B. A numerical investigation into the effects of Reynolds number on the flow mechanism induced by a tubercled leading edge. *Theor Comput Fluid Dyn* 2017; 31: 1–32.
30. Wei Z, New TH and Cui YD. Aerodynamic performance and surface flow structures of leading-edge tubercled tapered swept-back wings. *AIAA J* 2018; 56: 423–431.
31. Sudhakar S, Karthikeyan N and Venkatakrishnan L. Influence of leading edge tubercles on aerodynamic characteristics of a high aspect-ratio UAV. *Aerosp Sci Technol* 2017; 69: 281–289.
32. Heesu K, Jooha K and Haecheon C. Flow structure modifications by leading-edge tubercles on a 3D wing. *Bioinspir Biomimet* 2018; 13: 066011.
33. Post ML, Decker R, Sapell AR, et al. Effect of bio-inspired sinusoidal leading-edges on wings. *Aerosp Sci Technol* 2018; 81: 128–140.
34. Yasuda T, Fukui K, Matsuo K, et al. Effect of the Reynolds number on the performance of a NACA0012 wing with leading edge protuberance at low Reynolds numbers. *Flow Turbul Combust* 2019; 102: 435–455.
35. Mehraban AA, Djavareshkian MH, Sayegh Y, et al. Effects of smart flap on aerodynamic performance of sinusoidal leading-edge wings at low Reynolds numbers. *Proc IMechE, Part G: J Aerospace Engineering*. Epub ahead of print 4 August 2020. DOI: 10.1177/0954410020946903.
36. Esmaeilifar E, Djavareshkian MH, Forouzi Feshalami B, et al. Hydrodynamic simulation of an oscillating hydrofoil near free surface in critical unsteady parameter. *Ocean Eng* 2017; 141: 227–236.
37. Djavareshkian MH, Esmaeli A, Parsania A, et al. Three-dimensional investigation of smart flap aerodynamics for a WIG vehicle. *Trans Jpn Soc Aeronaut Space Sci Aerosp Technol Jpn* 2011; 9: 51–60.
38. Djavareshkian MH and Esmaeli A. Application of smart flap for race car wings. *Int J Aerodyn* 2012; 2: 66–92.
39. Djavareshkian MH, Esmaeli A and Parsani A. Aerodynamics of smart flap under ground effect. *Aerosp Sci Technol* 2011; 15: 642–652.
40. Johansson LC, Jakobsen L and Hedenström A. Flight in ground effect dramatically reduces aerodynamic costs in bats. *Curr Biol* 2018; 28: 3502–3507.
41. Jung KH, Chun HH and Kim HJ. Experimental investigation of wing-in-ground effect with a NACA6409 section. *J Mar Sci Technol* 2008; 13: 317–327.
42. Zhang MM, Wang GF and Xu JZ. Aerodynamic control of low-Reynolds-number airfoil with leading-edge protuberances. *AIAA J* 2013; 51: 1960–1971.
43. Zhang MM, Wang GF and Xu JZ. Experimental study of flow separation control on a low-Re airfoil using leading-edge protuberance method. *Exp Fluids* 2014; 55: 1710.
44. Sepahi-Younsi J, Forouzi Feshalami B, Maadi SR, Boundary layer suction for high-speed air intakes: a review. *Proc IMechE, Part G: J Aerospace Engineering* 2019; 233: 3459–3481 and Soltani MR.
45. Samiee A, Djavareshkian MH, Feshalami BF, et al. Improvement of airfoils aerodynamic efficiency by thermal camber phenomenon at low Reynolds number. *J Aerosp Technol Manag* 2018; 10: e4518.
46. Custodio D, Henoch CW and Johari H. Aerodynamic characteristics of finite span wings with leading-edge protuberances. *AIAA J* 2015; 53: 1878–1893.
47. Mueller TJ. *Aerodynamic measurements at low Reynolds numbers for fixed wing micro-air vehicles*. Notre Dame: Notre Dame University, Department of Aerospace and Mechanical Engineering, 2000.
48. Forouzi Feshalami B, Djavareshkian M, Zaree A, et al. The role of wing bending deflection in the aerodynamics of flapping micro aerial vehicles in hovering flight. *Proc IMechE, Part G: J Aerospace Engineering* 2019; 233: 3749–3761.
49. Forouzi Feshalami B, Djavareshkian M, Yousefi M, et al. Experimental investigation of flapping mechanism of the black-headed gull in forward flight. *Proc IMechE, Part G: J Aerospace Engineering* 2019; 233: 4333–4349.